Journal of Alloys and Compounds 614 (2014) 436–442

Contents lists available at ScienceDirect

Journal of Alloys and Compounds

journal homepage: www.elsevier.com/locate/jalcom

Magnetic and photocatalytic response of Ag-doped ZnFeO nano-composites for photocatalytic degradation of reactive dyes in aqueous solution

Asif Mahmood [a,*], Shahid Mahmood Ramay [b], Yousef S. Al-Zaghayer [a,c], Muhammad Imran [a], Shahid Atiq [d], Meshal S. Al-Johani [e]

[a] College of Engineering, Department of Chemical Engineering, King Saud University, Riyadh, Saudi Arabia
[b] College of Science, Department of Physics and Astronomy, King Saud University, Riyadh, Saudi Arabia
[c] Industrial Catalysts Research Chair, King Saud University, Riyadh 11421, Saudi Arabia
[d] Centre of Excellence in Solid State Physics, University of the Punjab, New Campus, Lahore 54590, Pakistan
[e] Energy Research Institute, King Abdulaziz City for Science and Technology (KACST), Riyadh 11442, Saudi Arabia

ARTICLE INFO

Article history:
Received 14 May 2014
Received in revised form 6 June 2014
Accepted 9 June 2014
Available online 27 June 2014

Keywords:
Photocatalyst
UV light
Methylene blue
Magnetic oxide
Water

ABSTRACT

To investigate the photocatalytic degradation of reactive dyes in aqueous solution, pure ZnO and Fe/Ag-doped magnetic photocatalysts having nominal compositions of $Zn_{0.95-x}Fe_{0.05}Ag_xO$ (x = 0.0, 0.05 and 0.1) have been synthesized via self-consistent sol–gel based auto-combustion route. Thermally stable samples were subsequently confirmed to exhibit wurtzite type hexagonal structure, characteristic of ZnO. The nature of chemical bonding was elaborated by Fourier transform analysis. Electron microscopic techniques were employed to investigate the structural morphology and to evaluate the particle size. Ferromagnetic nature of the Fe/Ag doped samples was revealed by vibrating sample magnetometry, enabling the photocatalytic samples to be re-collected magnetically for repeated usage. The enhanced photocatalytic activity in the degradation of methylene blue under UV light irradiation with 5 and 10 wt.% Ag/ZnFeO has been observed validating the potential applications of these materials in the field of photo-degradation of organic pollutants.

1. Introduction

Dilute magnetic semiconductor (DMS) materials have been attractive for spintronic devices due to their multiple functionalities and unique traits. Apart from various applications of these materials in advanced electronics such as opto-electronics, magneto-electronics, microwave devices, n/p-type doping and room temperature (RT) ferromagnetic characteristics, their photodegradation role for organic pollutants has recently been discovered [1–5]. Owing to its wide band gap (3.3 eV) and relatively large binding energy (60 meV) at RT, ZnO has emerged as a potential DMS material [6]. In addition to the wide range of optical and electronic applications such as solar cells, gas sensors, photocatalysis, ZnO-based DMS materials also demonstrate exceptional mechanical, thermal and chemical stability [7,8]. The use of ZnO-based photocatalysts is further motivated because of its high photosensitivity, high stability and non-toxic nature [9]. In addition, relatively large band gap value and higher ultraviolet (UV) light absorbing capability, also adds to its merits as promising catalyst for the degradation of organic pollutants as compared to TiO_2 [10].

Besides distinctive advantages of low cost and complete mineralization, photocatalysts used normally for degradation of organic pollutants are easily discharged in water which hinders their recovery and poses potential loss of material [11]. In this context, various solid–liquid separations based techniques such as centrifugation, ultra filtration and microfiltration have been practiced to separate suspended ZnO and TiO_2 photocatalytic particles [12–18]. On the other hand, magnetic photocatalysts assist the recovery of the photocatalysts from treated water by exploiting magnetic properties without compromising the activity and semiconducting properties [15,19,20].

Extensive studies have been carried out to convert ZnO from UV sensitive material to a visible-light irradiated material by doping elements like N, C, S, Co, Ag, Au, Pt and Ru [21–24]. Among these, Ag-doped ZnO have gained key focus due to its suitable functionalities as a photocatalyst, for the degradation of dyes [25–27]. This

* Corresponding author. Tel.: +966 11 4679966; fax: +966 11 4678770.
E-mail address: ahayat@ksu.edu.sa (A. Mahmood).

http://dx.doi.org/10.1016/j.jallcom.2014.06.055
0925-8388/

composition has been utilized for the generation of p-type conductivity wherein Ag ion acts as an electron acceptor in the material [15]. The improved photocatalytic activity of Ag-doped ZnO has been attributed to the dopant-mediated surface properties, such as oxygen vacancies and crystal defects [19]. On the other hand, Fe-doped ZnO has also been investigated for its potential photocatalytic activity for the degradation of organic dyes [4]. In this context, Ag/Fe co-doped ZnO could be a potential candidate to be exploited for the enhanced photocatalytic activity for the degradation of organic pollutants.

In this paper, we present the synthesis of Fe/ZnO dilute magnetic semiconductors doped with various Ag concentrations. The effect of Ag doping on the structural features, magnetic response and photocatalytic activity was investigated. The aim of the intended photocatalysts is to enhance the performance by the modification of surface texture. The degradation of methylene blue (MB) with the synthesized photocatalysts was investigated. The MB degradation behavior was examined using UV spectrophotometer.

2. Experimental procedure

2.1. Synthesis

Low cost sol–gel auto-combustion method was used to prepare pure ZnO and Ag-doped ZnFeO samples having compositions, $Zn_{0.95-x}Fe_{0.05}Ag_xO$ (x = 0.0, 0.05 and 0.1) [28]. Analytical grade reagents, zinc nitrate [$Zn(NO_3)\cdot 6H_2O$, ⩾99.0%, Sigma Aldrich], iron nitrate [$Fe(NO_3)_3\cdot 9H_2O$, ⩾99.999%, Sigma Aldrich] and silver nitrate [$AgNO_3$, 99.9999%, Sigma Aldrich] were used as starting materials in stoichiometric molar ratios while citric acid [$C_6H_8O_7$, ⩾99.5%, Sigma Aldrich] was used as a fuel agent. The metal nitrate to citric acid ratio [MN:CA] was adjusted to 1:2 for each sample. Precisely weighed amounts of these materials were first dissolved in 50 mL of deionized water and the solution was continuously stirred using a magnetic stirrer while placed on a hot plate. The temperature of the hot plate was fixed at 95 °C for about 1 h. Meanwhile, the solution was converted to a brownish xerogel. The stirrer was taken out of the gel at the instant and temperature was raised to 300 °C. After a few moments, the gel was burnt instantaneously with the evolution of gases and the final product was a loose and fluffy powder. The powder was then sintered at 400 °C for 2 h in a muffle furnace.

2.2. Characterization

Thermo gravimetric analysis (TGA) was carried out using an S-II, EXSTAR, Hitachi, TG/DTA at a temperature range of 35–750 °C, employing a heating rate of 9 °C/min in air. For structural analysis and phase identification, a Rigaku Ultimate IV, USA X-ray diffractometer (XRD) using Cu Kα radiation, was employed in the range of 25–70° with a step increment of 0.05°. Fourier transform infra-red (FT-IR) measurements were performed using a Bruker Vertex 70, Germany, spectrometer for analyzing the bonding characteristics of the prepared samples. Prior to this testing, the material was embedded in KBr. Structural morphology and elemental analysis was carried out by using a JEOL JSM7600F, FESM scanning electron microscope (SEM) attached with energy dispersive X-ray spectroscopy (EDS) from Oxford instruments.

The specific surface area, pore volume and average pore diameter of the catalysts were measured using a Micromeritics Tristar ASAP 2020, surface area and porosity analyzer by N_2 adsorption data at 77 K, according to the standard Brunauer Emmett Teller (BET) procedure. For each analysis, 0.25 g of catalyst was used. Prior to the analysis, degassing of the samples was carried out at 200 °C for 2 h to remove the moisture and weakly adsorbed gases from the catalyst surface. Transmission electron microscopy (TEM) studies was carried out by using JEOL 2100F, FEG-TEM, Japan.

The absorbance spectra were recorded on a Labomed-2950, USA UV absorbance spectrometer. UV diffuse reflectance spectroscopy measurements were carried out to calculate the energy band gaps (E_g) of the synthesized composites using Perkin Elmer's LAMBDA 35 UV systems with integrating sphere accessory. Magnetic properties were assessed by using a physical properties measurement system (PPMS, Quantum Design, USA) with a maximum applied field of ±10 kOe.

2.3. Photocatalytic activity measurements

In this study, MB was exploited as a pollutant molecule. The photocatalytic degradation of MB was carried out in a rectangular quartz reactor ($30 \times 40 \times 60$ mm^3). A MB aqueous solution (1.16×10^{-5} M) was photocatalyzed in a quartz reactor at RT under the UV light irradiation. In order to maintain the temperature of MB solution in the photo-reactor, cold water was circulated around the solution. A high-pressure mercury lamp (450 W, principal wavelength 365 nm and luminous intensity 0.4 mW cm^{-2}) served as the UV light source. 100 mg catalyst powders were dispersed into 100 mL MB aqueous solution (10 mg/L). Prior to irradiation, the suspension was sonicated in the dark to disperse the catalyst in dye solution and particular attention was given to the continuous stirring of the solution during the whole experiment. After irradiation at a given reaction time (0–4 h), about 2 mL of the mixed suspensions were extracted and filtered to separate the catalyst from the dye solution. The absorbance and degradation rates were determined by a UV spectrophotometer. The scanning wavelength range was from 400 to 800 nm.

3. Results and discussion

3.1. Thermal stability

TGA spectra were recorded to study the thermal degradation behavior of the as-synthesized samples in the temperature range of 35–750 °C, as shown in Fig. 1. The rapid initial weight loss observed is the characteristic of desorption/drying of water. The maximum weight loss in the observed temperature range was about 1% which could be attributed to the loss of residual water in the powder samples. No further degradation clearly demonstrates the thermal stability of the Ag-doped ZnFeO composite catalysts in this wide range of temperature.

3.2. Structural analysis

Fig. 2 shows the XRD patterns of pure (a) ZnO, (b) $Zn_{0.95}Fe_{0.05}O$ (ZnFeO), (c) 5 wt.% Ag/ZnFeO and (d) 10 wt.% Ag/ZnFeO samples obtained in the 2θ range of 25–70°. All the peaks present in the first two patterns have been identified as related to characteristic hexagonal wurtzite type structure of ZnO, since all the peaks are well-matched with JCPDS No. 75-1526, and hence indexed accordingly. No extra peaks corresponding to any secondary or impurity phase were observed in the patterns. The absence of any Fe-related peak in ZnFeO (Fig. 2(b)) might be attributed to two reasons. First, the substitution of dilute amount of Fe^{3+}, which had a smaller ionic radii (0.55 Å) as compared to the host Zn^{2+} (0.74 Å), could not distort the parent hexagonal matrix of ZnO [29]. The other may be attributed to the limitation of XRD technique to detect impurities present in very small amounts [3]. Fig. 2(c) and (d) reveals the XRD patterns of 5 and 10 wt.% Ag-doped ZnFeO, respectively. The patterns clearly demonstrate that along with ZnO peaks, three additional peaks related to Ag at 2θ values of 38.16°, 44.35° and 64.52° corresponding to (111), (200) and (220) planes, respectively, in accordance with JCPDS No. 04-0783, are also present.

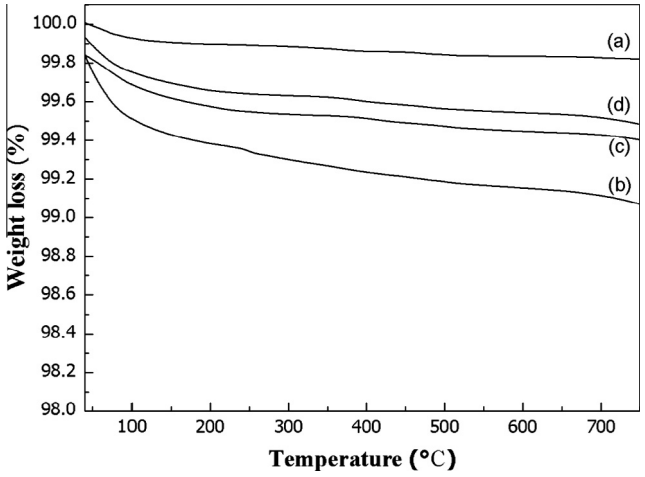

Fig. 1. Thermo gravimetric profiles of (a) ZnO, (b) $Zn_{0.95}Fe_{0.05}O$ (ZnFeO), (c) 5 wt.% Ag/ZnFeO, and (d) 10 wt.% Ag/ZnFeO.

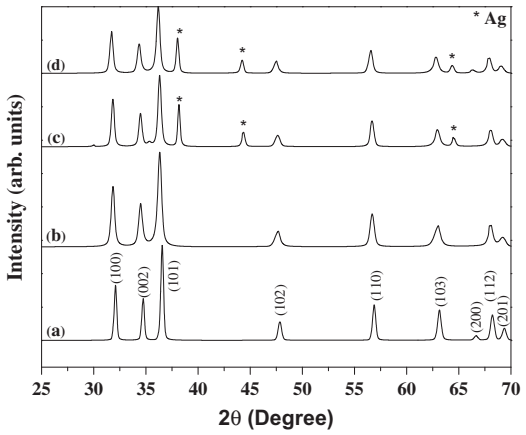

Fig. 2. XRD patterns of (a) ZnO, (b) $Zn_{0.95}Fe_{0.05}O$ (ZnFeO), (c) 5 wt.% Ag/ZnFeO, and (d) 10 wt.% Ag/ZnFeO.

Ag has not fully incorporated into the lattice of ZnFeO due to larger ionic radius of Ag as compared to Zn^{2+} and Fe^{3+} [30]. In addition, a slight and gradual perturbation was also observed in the diffraction peaks in all the four samples as shown in magnified patterns in Fig. 3. This shift in peak position towards left is mainly due to the presence of Fe in ZnO lattice [31].

The nature of chemical bonding in the synthesized un-doped and doped samples was studied using FTIR spectroscopy, as shown in Fig. 4. All the spectra showed two broad peaks at 3428 cm^{-1} and 1637 cm^{-1}, attributed to the surface-adsorbed water and OH-group, respectively [32]. The peaks at 2358 cm^{-1} and 1102 cm^{-1} are due to the presence of CO_2 in air and sulfate group, respectively [33,34]. The strongest peak in the range of 400–500 cm^{-1} is a characteristic peak of ZnO [31]. With the addition of 5% Fe in ZnO, the absorption band moved from 438 to 426 cm^{-1}. The change in the peak position of ZnO absorption band reveals that Zn–O–Zn network is perturbed by the presence of Fe in its lattice [31]. This observation is consistent with the magnified XRD spectrum shown in Fig. 3. Hence, it is inferred that Fe ions have replaced Zn ions and incorporated completely into the ZnO matrix. The FTIR spectra were further utilized to elaborate the effects of Ag-doping. No absorption peak related to AgO or Ag_2O was observed in the relevant spectra [35]. The absence of the Ag–oxide peaks could be attributed to the fact that Ag remained in metallic form and chemical bonding between Ag–O and Ag–ZnO could not occur [36].

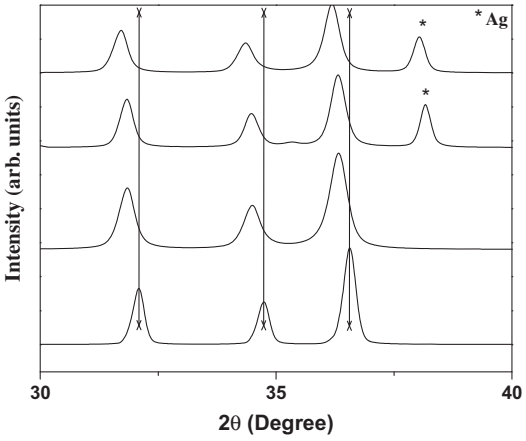

Fig. 3. Magnified XRD patterns of (a) ZnO, (b) $Zn_{0.95}Fe_{0.05}O$ (ZnFeO), (c) 5 wt.% Ag/ZnFeO, and (d) 10 wt.% Ag/ZnFeO.

The structural morphology of all the samples has been investigated by SEM as shown in Fig. 5(a–d). The grain sizes and grain boundaries could not be marked as the micrographs were taken at low resolution, however uniform distribution of small grains in the form of clusters is evident mainly in all the samples. The incorporation of Fe and Ag in ZnO has been observed to increase the surface roughness, porous nature with lots of channels and folds. In particular, after the addition of Ag, the surfaces became more rough and porous which might enhance the photocatalytic activity [9]. A porous structure can provide more surface contact and space to absorb the pollutant molecule to make the excited electron arrive more easily at the surface [37] and hence enhancing the photocatalytic activity. Furthermore, characteristic peaks recorded in the EDX spectra, shown in the insets of Fig. 5(a–d), elucidate the presence of Zn, Fe and Ag contents in accordance with the stoichiometric amounts as expected from the relevant sample composition.

Fig. 6 shows low-magnification TEM images of un-doped and Fe/Ag-doped ZnO samples. The particle size in case of pure ZnO and ZnFeO was almost same, in the average range of 50 nm. Whereas, it is observed that with the increase of Ag from 5 wt.% to10 wt.%, the average particle size decreases from about 40 to 30 nm on average. The reduced particle size favors an increase in surface to volume ratio of the nanoparticles which in turn increases the maximum utilization of the catalysts in the photocatalytical activity.

Specific surface area (BET), pore volume (PV) and average pore size (PD) of ZnO, ZnFeO and Ag-doped ZnFeO samples have been summarized in Table 1. The PV and PD were calculated from adsorption branch of the respective N_2 isotherm by applying Barrett, Joyner and Halenda (BJH) method. Moreover, it is also apparent from Table 1 that nanoparticle size confinement has a notable effect on textural properties, especially on pore volume, of the prepared catalysts. Ag-doped ZnFeO samples showed relatively higher specific surface area and pore volume than that of undoped sample. For instant, the BET surface area and pore volume of pristine sample were 4.97 m^2/g and 0.0196 cm^3/g, while for 10 wt.% Ag-doped samples both were 21.91 m^2/g and 0.214 cm^3/g, respectively which was in good agreement with the results determined by SEM and TEM.

3.3. Magnetic behavior

The magnetic properties of the synthesized samples except ZnO were investigated at a low temperature of 20 K. Fig. 7 shows the field-dependent magnetic hysteresis (M–H) loops obtained at an applied field of ±10 kOe. The saturation magnetizations (M_s) of $Zn_{0.95}Fe_{0.05}O$ was determined to be 1.72×10^{-4} which decreased to 7.70×10^{-5} emu/g for 10 wt.% Ag-doped sample, as listed in Table 1. The decreased value of M_s could be attributed to the doping of diamagnetic element Ag. Nevertheless, the overall ferromagnetic nature of the Ag-doped samples confirmed the utilization of these magnetic catalysts for use in photocatalytic activity for the photodegradation organic dyes.

3.4. Photocatalytic performance

The effect of Ag doping on the photocatalytic activity was assessed by evaluating the band gap and photo-absorption spectra technique. The energy band gap (E_g) of pure and doped samples was calculated using Eq. (1) [38].

$$\alpha h\upsilon = A(h\upsilon - E_g)^{n/2} \quad (1)$$

where α, υ, E_g and A are absorption coefficient, light frequency, band gap energy, and a constant, respectively, and n is based on the

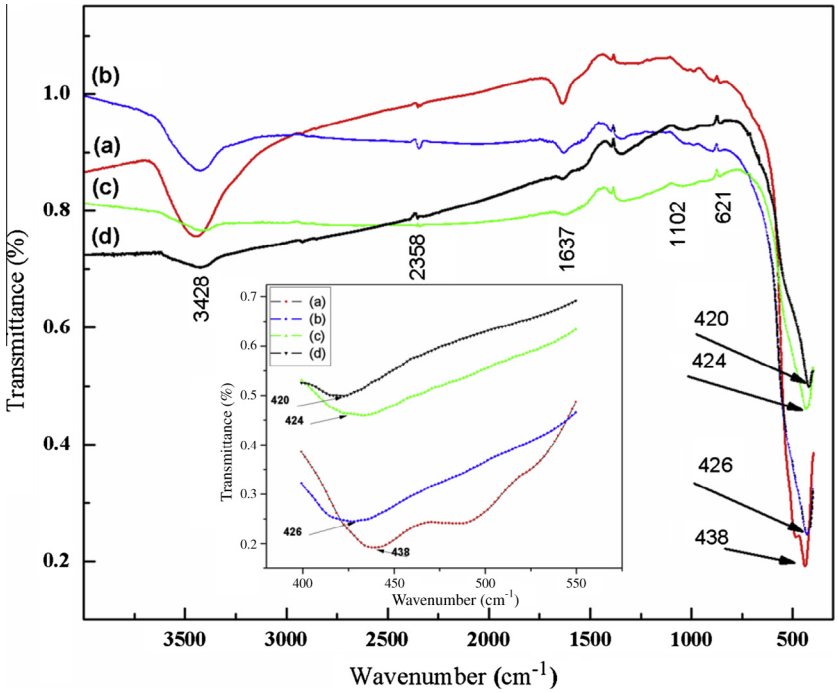

Fig. 4. FTIR spectra of (a) ZnO, (b) $Zn_{0.95}Fe_{0.05}O$ (ZnFeO), (c) 5 wt.% Ag/ZnFeO, and (d) 10 wt.% Ag/ZnFeO.

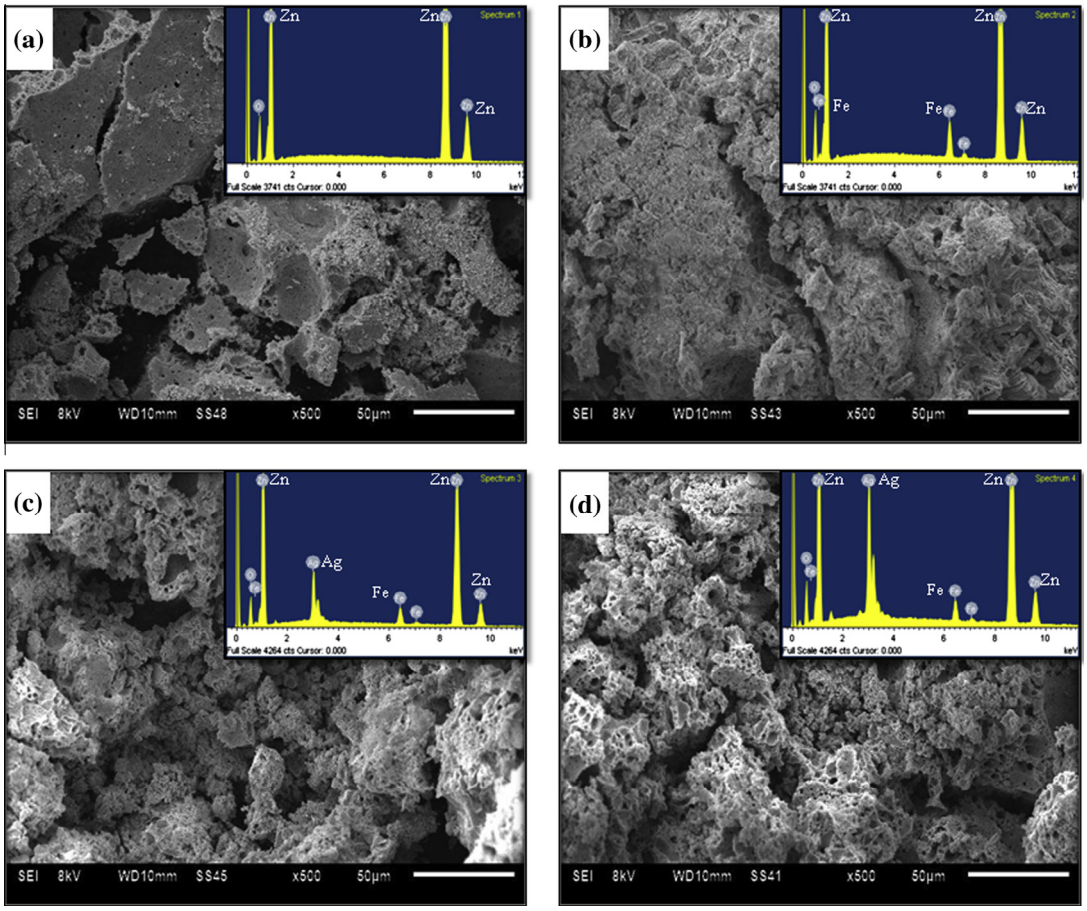

Fig. 5. SEM micrographs of (a) ZnO, (b) $Zn_{0.95}Fe_{0.05}O$ (ZnFeO), (c) 5 wt.% Ag/ZnFeO, and (d) 10 wt.% Ag/ZnFeO, and the relevant EDX spectra in the insets.

nature of optical transition of a semiconductor. For example, $n = 1$ stands for direct transition, whereas $n = 4$ stands for indirect transition. The calculated band gap energy of Ag-doped samples was decreased as compared to un-doped sample (Table 1). The surface

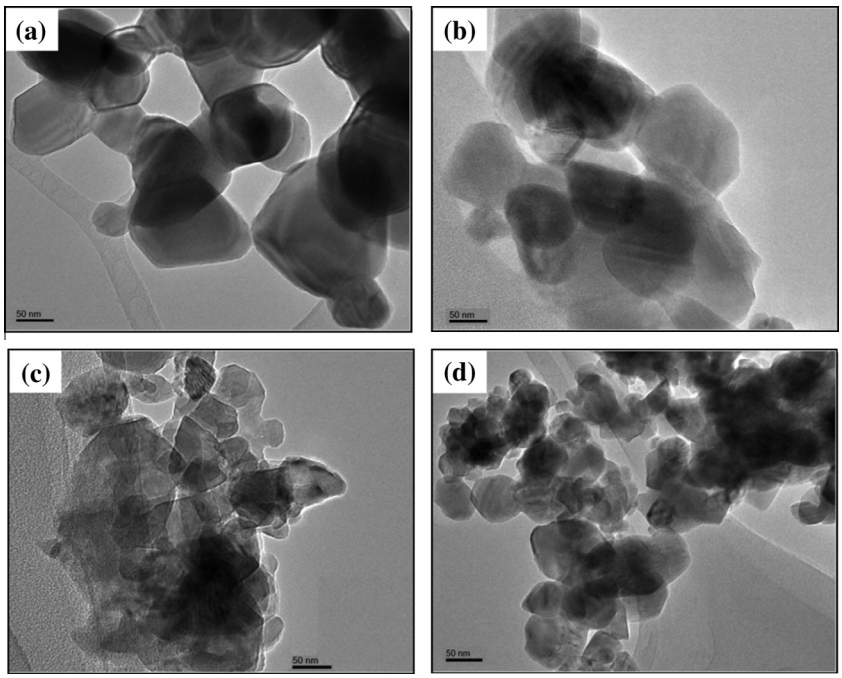

Fig. 6. Low-magnification TEM images of (a) ZnO, (b) $Zn_{0.95}Fe_{0.05}O$ (ZnFeO), (c) 5 wt.% Ag/ZnFeO, and (d) 10 wt.% Ag/ZnFeO.

Table 1
Textural properties, band-gap energies and saturation magnetization of the un-doped and Ag-doped ZnFeO catalysts.

Samples	Surface area (m^2/g)	Pore volume (cm^3/g)	Average pore size (nm)	Band gap energy (eV)	Saturation magnetization (M_s) (emu/g)
ZnO	4.97	0.0196	19.71	3.22	–
ZnFeO	16.45	0.111	29.58	3.17	1.72×10^{-4}
5 wt.% Ag/ZnFeO	18.04	0.190	31.79	3.15	7.74×10^{-5}
10 wt.% Ag/ZnFeO	21.91	0.214	34.57	3.14	7.70×10^{-5}

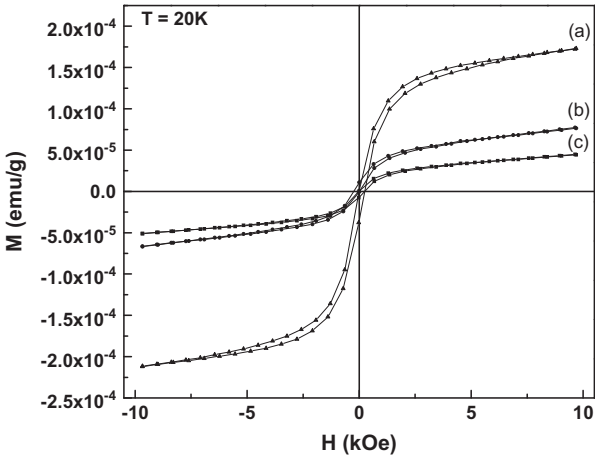

Fig. 7. Field-dependent *M–H* loops of (a) $Zn_{0.95}Fe_{0.05}O$ (ZnFeO), (b) 5 wt.% Ag/ZnFeO, and (c) 10 wt.% Ag/ZnFeO.

modification with Ag doping can cause a red-shift of around 0.04 eV [8]. The decrease in band gap energy of Ag-doped samples may be due to the band shrinkage effect [39]. Fig. 8 shows a plot between $(\alpha h\upsilon)^{1/2}$ and $h\upsilon$. The sharp tangents were drawn to determine the band gaps of the synthesized catalysts. The value of band gap was reduced gradually from 3.22 to 3.14 eV starting from the ZnO to 10 wt.% Ag/ZnFeO sample as summarized in Table 1.

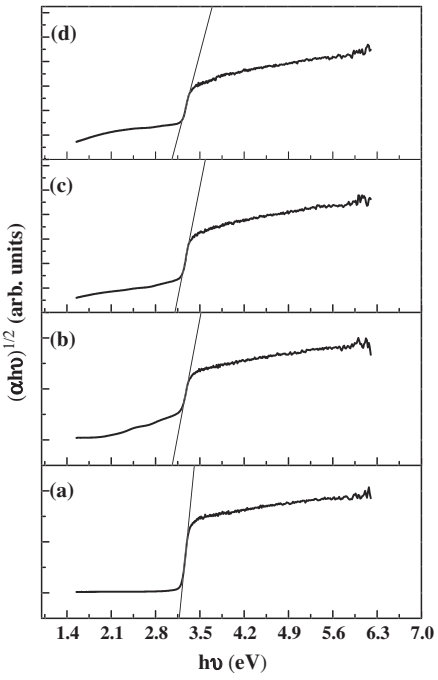

Fig. 8. $(\alpha h\upsilon)^{1/2}$ vs. photon energy $(h\upsilon)$ for (a) ZnO, (b) $Zn_{0.95}Fe_{0.05}O$ (ZnFeO), (c) 5 wt.% Ag/ZnFeO, and (d) 10 wt.% Ag/ZnFeO.

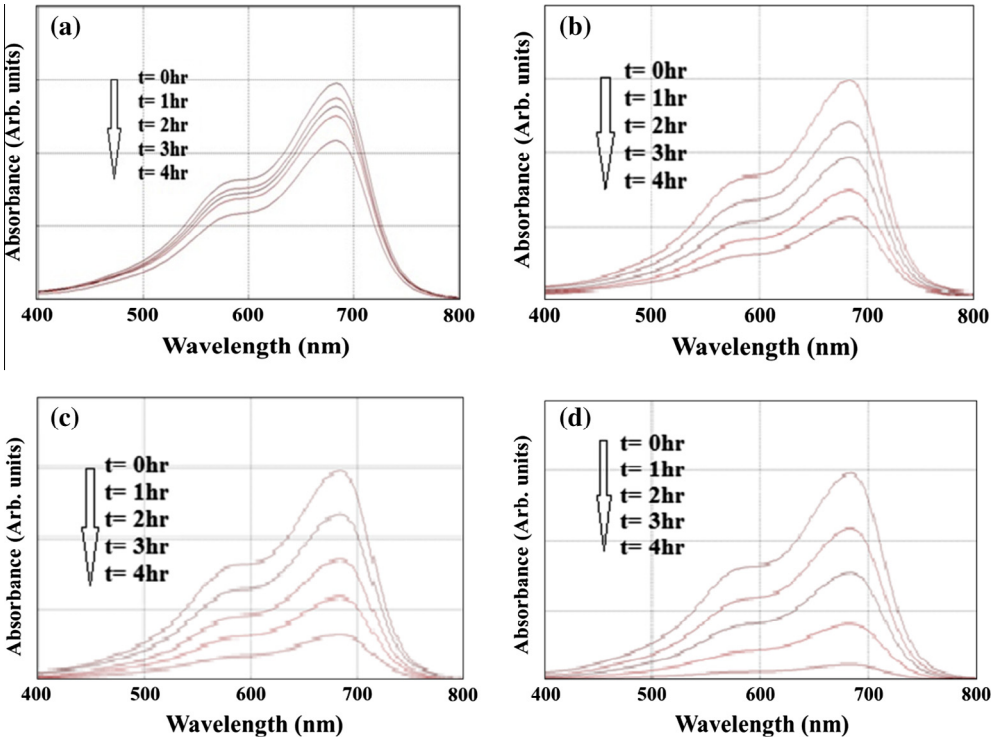

Fig. 9. Time-dependent UV absorption spectra of (a) ZnO, (b) $Zn_{0.95}Fe_{0.05}O$ (ZnFeO), (c) 5 wt.% Ag/ZnFeO, and (d) 10 wt.% Ag/ZnFeO.

UV–Vis spectroscopy analyses were performed to determine the effect of Ag-doping on the optical properties of the ZnO nanoparticles. Fig. 9 shows the photoabsorption spectra of the degraded dye solutions with respect to light-exposure durations ranging from 0 to 4 h. It was clearly evident that the absorption of MB gradually decreased with increasing irradiation time; however, different values of the degree of reduction were observed for each catalyst. The least degradation of around 35% was observed after illuminating the solution for 4 min under UV light that could be seen in Fig. 9(a). After incorporating Ag in the same sample, the MB showed a promising degradation of about 87% after 4 h exposure to UV light, as exhibited in Fig. 9(d). It can be seen that the maximum absorbance at 665 nm rapidly decreases with the increase in irradiation time and disappears almost completely after a certain time.

The incorporation of Ag may expedite the transport of photogenerated electrons, facilitating the longer charge separation by trapping them, which results in a positive effect on the MB degradation [25,28].

The order of catalytic activity for MB degradation with the as-synthesized catalysts is 10 wt.% Ag/ZnFeO > 5 wt.% Ag/ZnFeO > ZnFeO > ZnO which is consistent with the order of band gaps (Table 1) of these materials. The decreased band gap by incorporating Fe and Ag in ZnO lattice demonstrates the effectiveness of the resulting materials for MB degradation in the UV light irradiation. Based upon experimental observations, it is elucidated that the degradation of MB increases by increasing irradiation time under UV light in the presence of photocatalysts due to increase in life time of excited charge carriers which may enhance the photocatalytic activities [40].

4. Conclusions

In this article, pure ZnO, Fe-doped ZnO, and Ag-doped ZnFeO were synthesized via self-consistent sol–gel based auto-combustion method. The XRD analysis showed that Fe incorporation in ZnO did not distort the wurtzite ZnO structure while Ag loading in ZnFeO resulted in phase separation (yielding Ag-doped ZnFeO nano-composites). Ferromagnetic behavior was evident for the doped samples enabling the photocatalysts to be re-collected and re-used multiple times. The UV diffuse reflectance spectroscopy displayed the decreased value of band gaps by the addition of Fe in ZnO which were further decreased by adding Ag in ZnFeO. An organic dye (methylene blue) was chosen as a model component which was degraded under UV light irradiation. The results revealed that the minimum degradation of MB had taken place with pure ZnO which was increased by adding Fe into ZnO lattice. The degradation of MB was further increased by incorporating Ag into ZnFeO. The increase in dye degradation was attributed to the increased life time of excited charge carriers, reduced recombination of electron–hole pairs, and decrease in materials band gaps by the addition of Fe and Ag in ZnO.

Acknowledgement

The Authors extend their appreciation to the Deanship of Scientific Research at King Saud University for funding the work through the research group Project No. RGP-VPP-311.

References

[1] S.W. Jung, S.J. An, G.C. Yi, C.U. Jung, S.I. Lee, S. Cho, Appl. Phys. Lett. 80 (2002) 4561–4563.
[2] H. Ohno, Science 281 (1998) 951–956.
[3] B.S. Reddy, S.V. Reddy, N.K. Reddy, Y.P. Reddy, Adv. Mater. Lett. 5 (2014) 199–205.
[4] S.J. Pearton, D.P. Norton, K. Ip, Y.W. Heo, T. Steiner, J. Vac. Sci. Technol. B 22 (2004) 932–948.
[5] S. Dong, K. Xu, J. Liu, H. Cui, Physica B 406 (2011) 3609–3612.
[6] A. Goktas, I.H. Mutlu, Y. Yamada, Superlattice Microstruct. 57 (2013) 139–149.
[7] A. Mclaren, T.V. Solis, G. Li, S.C. Tsang, J. Am. Chem. Soc. 131 (2009) 12540–12541.
[8] O.A. Yildirim, H.E. Unalan, C. Durucan, J. Am. Ceram. Soc. 96 (2013) 766–773.
[9] S.T. Hung, C.J. Chang, M.H. Hsu, J. Hazard. Mater. 198 (2011) 307–316.

[10] S. Sakthivel, B. Neppolian, M.V. Shankar, B. Arabindoo, M. Palanichamy, V. Murugesan, Sol. Energy Mater. Sol C 77 (2003) 65–82.
[11] R. Wang, D. Xu, J.B. Liu, K.W. Li, H. Wang, Chem. Eng. J. 168 (2011) 455–460.
[12] R.J. Watts, S. Kong, W. Lee, J. Environ. Eng.-ASCE 7 (1995) 730–735.
[13] S. Kagaya, K. Shimizu, R. Arai, K. Hasegawa, Water Res. 33 (1999) 1753–1755.
[14] T.N. Angelidis, M. Koutlemani, I. Poulios, Appl. Catal. B-Environ. 16 (1998) 347–357.
[15] J.M. Herrmann, J. Disdier, P. Pichat, S. Malato, J. Blanco, Appl. Catal. B-Environ. 17 (1998) 15–23.
[16] R.C. Suciu, I. Marian, I. Bratu, J. Alloys Comp. 584 (2014) 159–166.
[17] Q. Wang, H. Jiang, S. Zang, J. Li, Q. Wang, J. Alloys Comp. 586 (2014) 411–419.
[18] S. Paul, P. Chetri, A. Choudhury, J. Alloys Comp. 583 (2014) 578–586.
[19] S.Q. Liu, Environ. Chem. Lett. 10 (2012) 209–216.
[20] S. Rehman, R. Ullah, A.M. Butt, N.D. Gohar, J. Hazard. Mater. 170 (2009) 560–569.
[21] E. Casbeer, V.K. Sharma, X.Z. Li, Sep. Purif. Technol. 87 (2012) 1–14.
[22] S. Boumaza, A. Boudjemaa, A. Bouguelia, R. Bouarab, M. Trari, Appl. Energy 87 (2010) 2230–2236.
[23] S. Ida, K. Yamada, T. Matsunaga, H. Hagiwara, Y. Matsumoto, T. Ishihara, J. Am. Chem. Soc. 132 (2010) 17343–17345.
[24] R. Dom, R. Subasri, K. Radha, P.H. Borse, Solid State Commun. 151 (2011) 470–473.
[25] P.V. Korake, R. Sridharkrishna, P.P. Hankare, K.M. Garadkar, Toxicol. Environ. Chem. 94 (2012) 1075–1085.
[26] R. Wang, J.H. Xin, Y. Yang, H. Liu, L. Xu, J. Hu, Appl. Surf. Sci. 227 (2004) 312–317.
[27] M.A. Behnajady, N. Modirshahla, M. Shokri, A. Zeininezhad, H.A. Zamani, J. Environ. Sci. Health A 44 (2009) 666–672.
[28] K.C. Patil, S.T. Aruna, T. Mimani, Curr. Opin. Solid State Mater. 6 (2002) 507–512.
[29] Z. Bin, Z.S. Min, W.H. Wei, D.Z. Liang, Chin. Sci. Bull. 53 (2008) 1639–1643.
[30] R.D. Shannon, Acta Crystallogr. A 32 (1976) 751–767.
[31] S. Kumar, S. Gautam, Y.J. Kim, B.H. Koo, K.H. Chae, C.J. Lee, J. Ceram. Soc. Jpn. 117 (2009) 616–618.
[32] S.C. Pillai, P. Periyaat, R. George, D.E. McCormack, M.K. Seery, H. Hayaden, J. Colreavy, D. Corr, S.J. Hinder, J. Phys. Chem. C 111 (2007) 1605–1611.
[33] T. Rattana, S. Suwanboon, P. Amornpitoksuk, A. Haidoux, P. Limsuwan, J. Alloys Compd. 480 (2009) 603–607.
[34] C.K. Srikanth, P. Jeevanandam, J. Alloys Compd. 486 (2009) 677–684.
[35] J. Das, D. Khushalani, J. Phys. Chem. C 114 (2010) 2544–2550.
[36] G.I.N. Waterhouse, G.A. Bowmaker, J.B. Metson, Phys. Chem. Chem. Phys. 3 (2001) 3838–3845.
[37] X. Duan, R. Gao, Y. Zhang, Z. Jian, Mater. Lett. 65 (2011) 3625–3628.
[38] C. Liu, H. Lin, S. Gao, P. Yin, L. Guo, B. Huang, Y. Dai, B. Kor, Chem. Soc. 35 (2014) 441–447.
[39] K. Ranjan, A. Sahu, K. Ganguly, M. Mishra, R.S. Ningthoujam, J. Colloid Interface Sci. 366 (2012) 8–15.
[40] M. Saleem, S.A. Siddiqi, S.M. Ramay, S. Atiq, S. Naseem, Chin. Phys. Lett. 29 (2012). 106103-3.